Journal of Physics: Conference Series **441** (2013) 012009 doi:10.1088/1742-6596/441/1/012009

Transport characteristics of $N_2(A^3\Sigma_u^+)$, $N(^4S^o)$, and $N(^2D^o)$ in a remote nitrogen plasma source

Y Horikawa[1], T Hayashi[2], and K Sasaki[3]

[1]Department of Quantum Science and Engineering, Graduate School of Engineering, Hokkaido University, Sapporo 060-8628, Japan
[2]Plasma Nanotechnology Research Center, Nagoya University, Nagoya 464-8603, Japan
[3]Division of Quantum Science and Engineering, Faculty of Engineering, Hokkaido University, Sapporo 060-8628, Japan

E-mail: horikawa@athena.qe.eng.hokudai.ac.jp

Abstract. We measured absolute densities of $N_2(A^3\Sigma_u^+)$, $N(^4S^o)$, and $N(^2D^o)$ in the downstream region at various distances from a microwave N_2 plasma source. As a result, it was found that the transport of $N(^4S^o)$ was highly efficient with keeping the densities on the order of 10^{17} m^{-3} at distances up to 12 cm from the discharge region. On the other hand, the densities of $N_2(A^3\Sigma_u^+)$ and $N(^2D^o)$ decayed from 10^{16} to 10^{14} m^{-3} when the distance between the discharge region and the measurement position was lengthened from 6 to 12 cm. The decay curves of the $N_2(A^3\Sigma_u^+)$ and $N(^2D^o)$ densities were different each other. The densities of $N_2(A^3\Sigma_u^+)$ and $N(^2D^o)$ in the downstream region were not owing to the transports but were due to their productions. We discussed the dominant production processes of $N_2(A^3\Sigma_u^+)$ and $N(^2D^o)$ on the basis of the experimental observations.

1. Introduction

Plasma-based reactive ion etching (RIE) [1] is a key technology in the fabrication of ultralarge-scale integrated circuits. However, RIE sometimes causes serious problems in the processing step where plasma-induced damage must be avoided. A mechanism of plasma-induced damage is the bombardment of energetic ions onto the wafer [2]. Using a remote plasma source is a conventional method for avoiding plasma-induced damage caused by ion bombardment. Recently, a new method for damage-less dry etching of silicon using a remote plasma has been reported [3]. In this method, NF_3 is fed into the downstream region of a remote nitrogen plasma source, where the density and the energy of ions are much lower than those in an active plasma. The dry etching of silicon indicates that NF_3 is dissociated into F atoms in the downstream region of the N_2 remote plasma. A question here is the dissociation mechanism of NF_3. A molecular orbital calculation suggests that atomic nitrogen at the metastable $^2D^o$ state and molecular nitrogen at the metastable $A^3\Sigma_u^+$ state can dissociate NF_3 into F atoms, while the collision with atomic nitrogen at the ground state ($^4S^o$) does not result in the production of F atoms [3]. However, the transport characteristics of the metastable states to the downstream region of a remote plasma source have not yet been examined.

In this paper, we measured the densities of $N_2(A^3\Sigma_u^+)$, $N(^4S^o)$, and $N(^2D^o)$ in the downstream region of a remote N_2 plasma source. To compare the absolute densities of the above species, we employed cavity ringdown spectroscopy (CRDS) for measuring the $N_2(A^3\Sigma_u^+)$ density and vacuum ultraviolet absorption spectroscopy (VUVAS) for measuring the $N(^4S^o)$ and $N(^2D^o)$ densities. The measurements were carried out at various distances from the discharge region. The experimental results give us useful

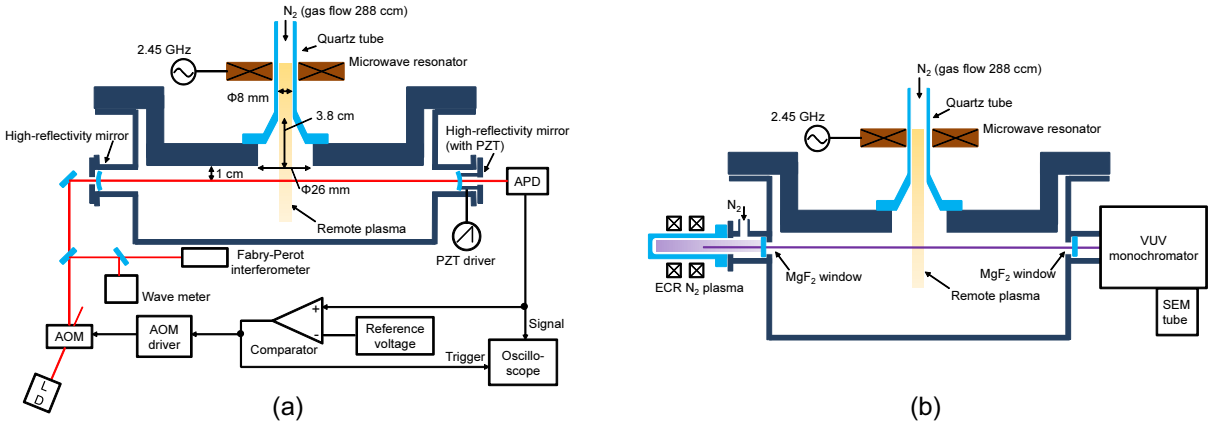

Figure 1. Experimental apparatus for measuring (a) the $N_2(A^3\Sigma_u^+)$ density by cavity ringdown spectroscopy and (b) the $N(^4S^o)$ and $N(^2D^o)$ densities by vacuum ultraviolet absorption spectroscopy in the downstream region of a remote N_2 plasma source.

information for the optimum discharge condition of the remote N_2 plasma to realize high densities of $N_2(A^3\Sigma_u^+)$ and $N(^2D^o)$ in the downstream region.

2. Experimental apparatus

Figure 1 shows the schematic illustrations of the experimental apparatus. Pure N_2 plasmas were produced in a quartz tube by surfatron discharge. The power source was a magnetron generator at a frequency of 2.45 GHz. The magnetron generator was connected to a microwave resonator via an isolator, a power monitor, a stub tuner, and a convertor from rectangular to coaxial waveguides. The microwave power was set at 100 W. The quartz tube with an inner diameter of 8 mm passed through the hole at the center of the microwave resonator. N_2 gas was fed from the top of the quartz tube at a flow rate of 288 ccm. The length of the active discharge region along the quartz tube was dependent on the discharge conditions, and was roughly 1.5 - 2 cm. The quartz tube was connected to a stainless-steel cylindrical chamber with a diameter of 30 cm, where spectroscopic systems for measuring the densities of $N_2(A^3\Sigma_u^+)$, $N(^4S^o)$, and $N(^2D^o)$ were installed. The cylindrical chamber had a hole of 26 mm in diameter on the top plate, and the spatial afterglow of the N_2 plasma was introduced into the chamber via the hole. The microwave resonator was movable, and the following measurements were carried out in the spatial afterglow at various distances from the active discharge region.

The $N_2(A^3\Sigma_u^+)$ density was measured by CRDS as shown in figure 1(a). The details of the CRDS system have previously been reported [4]. Briefly, the spatial afterglow of the N_2 plasma was sandwiched by an optical cavity which was composed of two concave mirrors with high reflectivities. The cavity length was 1 m. We injected a cw diode laser beam into the cavity via an acousto-optic modulator (AOM), and detected the laser intensity transmitted through the cavity. The wavelength of the laser was tuned at around 771.100 nm, which corresponded to the $B^3\Pi_g(v'=2)-A^3\Sigma_u(v''=0)$ absorption band of N_2. The rapid truncation of the laser beam, by triggering AOM at the moment when the cavity length was resonant with the laser wavelength, resulted in an exponential decay of the transmitted laser intensity. And the $N_2(A^3\Sigma_u^+)$ density was deduced from the decay time constant (the ringdown time).

The densities of $N(^4S^o)$ and $N(^2D^o)$ were measured by VUVAS as shown in figure 1(b). The details of the VUVAS system have also been reported elsewhere [5, 6]. In brief, the spatial afterglow of the N_2 plasma was placed between an electron cyclotron resonance N_2 plasma (the light source) and a VUV monochromator. Two MgF_2 windows were used for separating the cylindrical chamber, the light source plasma, and the VUV monochromator. The intensities of line emissions yielded from the light source plasma were detected using a secondary-electron multiplier tube via the VUV monochromator. The

N($^4S^o$) and N($^2D^o$) densities were deduced from the absorption strengths of the $^4S^o - ^4P$ (120.0 nm) and $^2D^o - ^2D$ (124.3 nm) transitions, respectively.

Both the absorption chords of CRDS and VUVAS were located at a distance of 1 cm from the top plate of the chamber. In addition to the absorption measurements, we carried out conventional optical emission spectroscopy using a spectrograph with a focal length of 50 cm and a grating of 600 grooves/mm. The measurement position was 4.8 cm distant from the end of the quartz tube.

3. Results and Discussion

Figures 2 and 3 show the densities of $N_2(A^3\Sigma_u^+)$, N($^4S^o$) and N($^2D^o$), the gas temperature, and the optical emission intensities of the first positive (N_2), the second positive (N_2), and the first negative (N_2^+) bands. These results were obtained at pressures of 0.5 (figure 2) and 7 Torr (figure 3) at various distances from the discharge region. The origin of the distance from the discharge region (the z axis) is defined as the bottom-side edge of the microwave resonator. The densities of $N_2(A^3\Sigma_u^+)$, N($^4S^o$) and N($^2D^o$) were estimated from their line-integrated densities on the assumption of the absorption length as 30 cm (the diameter of the cylindrical chamber). The gas temperature was evaluated by fitting the absorption spectrum of the $B^3\Pi_g(v' = 2) - A^3\Sigma_u(v'' = 0)$ transition with the theoretical one which was calculated by assuming the same values for the rotational and translational temperatures (the Doppler broadening). The error bars shown in figure 3(b) indicate the ambiguity in the evaluation of the gas temperature by the spectral fitting. The optical emission intensities plotted in figures 2(c) and 3(c) were obtained by integrating the band spectra along the wavelength.

As shown in figures 2(a) and 3(a), the density of N($^4S^o$) was much higher than the densities of $N_2(A^3\Sigma_u^+)$ and N($^2D^o$). A higher N($^4S^o$) density was observed at a higher gas pressure. The decay of the N($^4S^o$) density with distance from the discharge region was negligibly small, keeping the density on the order of 10^{17} m^{-3} at both the pressures of 0.5 and 7 Torr. This result indicates the negligible destruction of N($^4S^o$) in the gas phase [7] as well as on the surface of the quartz tube [8]. Accordingly, the lifetime of N($^4S^o$) was sufficiently long to be transported from the discharge to downstream regions. Although the production of N($^4S^o$) would be expected in the downstream region due to a similar mechanism to those described below, it can be considered that the N($^4S^o$) density in the downstream region is dominated by the transport from the active discharge region.

The principal subject of this paper is the transport characteristics of $N_2(A^3\Sigma_u^+)$ and N($^2D^o$), since the efficient transport of N($^4S^o$) does not contribute to dissociation of NF_3 according to the molecular orbital calculation [3]. The destructions of $N_2(A^3\Sigma_u^+)$ and N($^2D^o$) occur both in the gas phase [9–11] and on the surface of the quartz tube. In general, the surface loss probabilities of electronic-excited metastable states are believed to be equal to unity. Although several works reported possibilities that the surface loss probabilities on dielectric surfaces are less than unity ($\alpha = 0.11$ [12] and $\alpha \geq 0.25$ [13] for He*($^3S_1$), $0.5 < \alpha < 0.85$ [13], $\alpha \simeq 0.7$ [14], and $\alpha \simeq 0.72$ [15] for Ar*(^3P), and $\alpha \geq 0.75$ for Xe*($^3P_2$) [13]), it is unlikely that a surface loss probability is much smaller than unity. When we assume a surface loss probability of unity, the diffusion lifetimes of $N_2(A^3\Sigma_u^+)$ and N($^2D^o$) in the quartz tube are estimated to be 10 and 8 μs, respectively, according to their diffusion coefficients reported in literatures [16, 17]. The diffusion lifetimes correspond to the transport lengths of $v_f\tau_D = 9$ and 7 μm in the quartz tube, where τ_D and v_f are the diffusion lifetime and the flow speed of N_2, respectively. Therefore, even though the laminar gas flow avoids the frequent arrivals on the surface of the quartz tube, it is impossible to expect the transport length of several centimeters for $N_2(A^3\Sigma_u^+)$ and N($^2D^o$).

As shown in figures 2(a) and 3(a), the densities of $N_2(A^3\Sigma_u^+)$ and N($^2D^o$) were much lower than the N($^4S^o$) density in the downstream region. Having had considered the experimental result we reported previously [18], it would be expected that the densities of $N_2(A^3\Sigma_u^+)$, N($^4S^o$), and N($^2D^o$) are on a similar order of magnitude in the active discharge region at a pressure of 0.5 Torr. Hence, the lower $N_2(A^3\Sigma_u^+)$ and N($^2D^o$) densities than the N($^4S^o$) density suggest losses of $N_2(A^3\Sigma_u^+)$ and N($^2D^o$) during their transport. The decays of the $N_2(A^3\Sigma_u^+)$ and N($^2D^o$) densities with the distance from the discharge region also suggest their losses during their transport. However, as described in the previous paragraph,

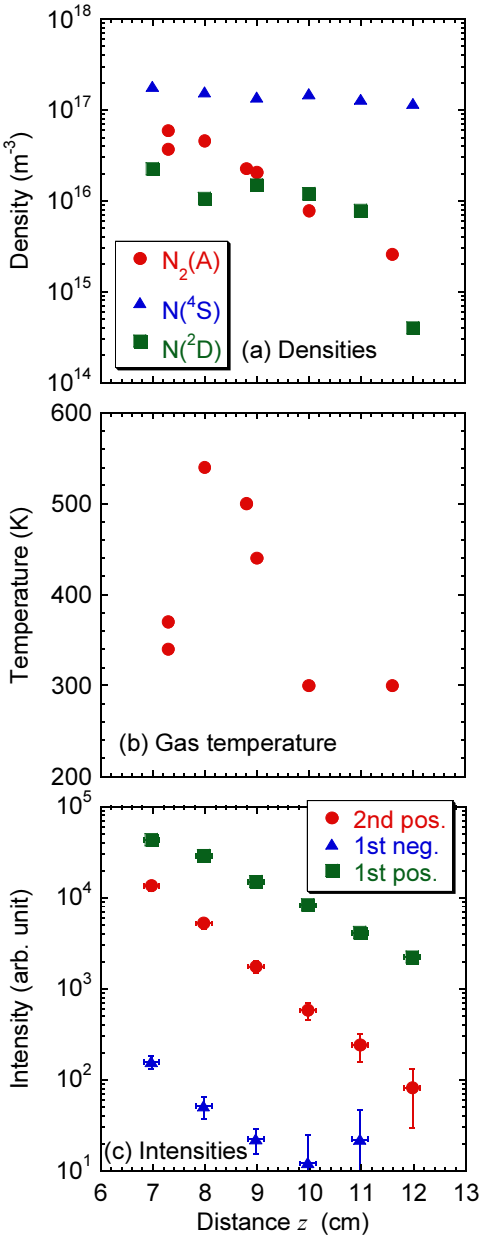

Figure 2. Densities of $N_2(A^3\Sigma_u^+)$, $N(^4S^o)$, and $N(^2D^o)$, the gas temperature, and the optical emission intensities observed in the downstream region of a N_2 remote plasma produced at a pressure of 0.5 Torr.

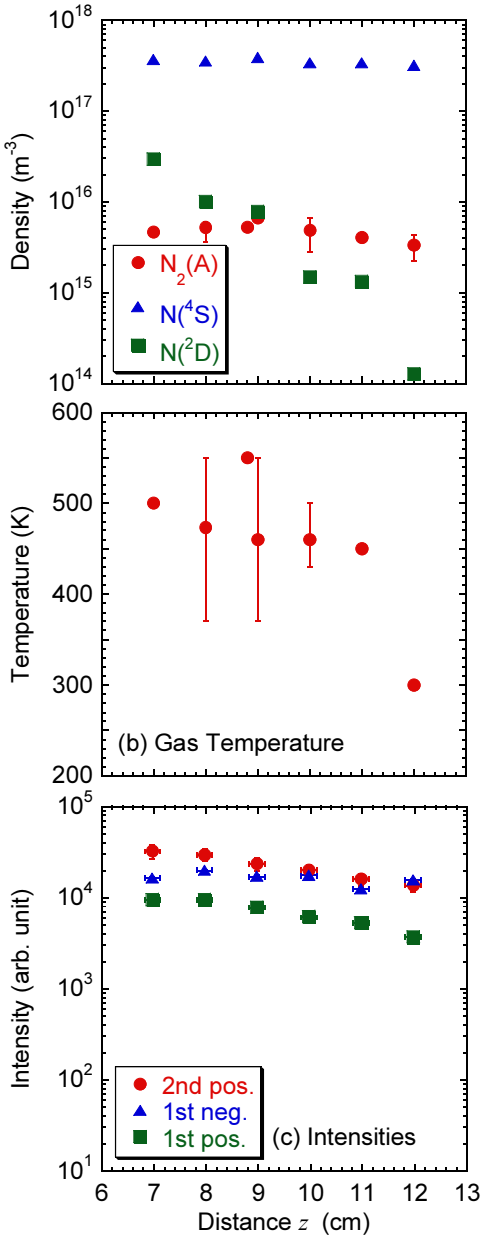

Figure 3. Densities of $N_2(A^3\Sigma_u^+)$, $N(^4S^o)$, and $N(^2D^o)$, the gas temperature, and the optical emission intensities observed in the downstream region of a N_2 remote plasma produced at a pressure of 7 Torr.

the transportation lengths of $N_2(A^3\Sigma_u^+)$ and $N(^2D^o)$ are expected to be short, and the experimentally-observed densities on the order of 10^{15} m^{-3} at a distance of 10 cm from the discharge region cannot be explained by the transport. In other words, the $N_2(A^3\Sigma_u^+)$ and $N(^2D^o)$ densities observed experimentally suggest their productions outside the active discharge region.

The productions of $N_2(A^3\Sigma_u^+)$ and $N(^2D^o)$ are supported by the observations of the optical emission

intensities in the downstream region, as shown in figures 2(c) and 3(c). It is noted that no optical emission intensities were observed in the downstream region at a distance of $z \geq 6$ cm from the discharge region, when we employed argon for the discharge. This indicates that the downstream region shown in figures 2 and 3 is the outside of the active discharge region. In contrast, when we employed nitrogen for the discharge, we observed optical emission intensities of the first positive, the second positive, and the first negative bands in the downstream region, which indicate the productions of $N_2(B^3\Pi_g)$, $N_2(C^3\Pi_u)$, and $N_2^+(B^2\Sigma_u^+)$ states, respectively. In addition, we observed gas heating as shown in figures 2(b) ($8 \leq z \leq 9$ cm), which suggests that a kind of power deposition is available in the downstream region.

The production of $N_2(A^3\Sigma_u^+)$ in the flowing afterglow has been investigated intensively by Sadeghi *et al.* (experimentally) [19] and Guerra *et al.* (theoretically) [20]. Guerra and coworkers pointed out the possibility of energy transport to the downstream region by ground-state molecular nitrogen at highly-excited vibrational states. Highly-excited vibrational states are populated by the V-V pumping-up mechanism,

$$N_2(X^1\Sigma_g^+, v) + N_2(X^1\Sigma_g^+, w) \rightarrow N_2(X^1\Sigma_g^+, v+1) + N_2(X^1\Sigma_g^+, w-1). \quad (1)$$

Highly-excited vibrational states thus formed contribute to the production of $N_2(A^3\Sigma_u^+)$ via reactions

$$N_2(X^1\Sigma_g^+, v \geq 10) + N(^2P) \rightarrow N_2(A^3\Sigma_u^+) + N(^4S) \quad (2)$$

and

$$N_2(X^1\Sigma_g^+, v \geq 39) + N(^4S) \rightarrow N_2(A^3\Sigma_u^+) + N(^2D^o). \quad (3)$$

In addition, since the observation of the optical emission intensity at the first negative system of N_2^+ suggests the existence of electrons, electron impact excitation

$$N_2(X^1\Sigma_g^+, v) + e \rightarrow N_2(A^3\Sigma_u^+) + e \quad (4)$$

may partly contribute to the production of $N_2(A^3\Sigma_u^+)$, if electrons are considerably heated in the downstream region. Guerra and coworkers pointed out the importance of $N_2(X^1\Sigma_g^+, v \geq 25)$ as the parent of $N_2(A^3\Sigma_u^+)$ in reaction (4) because of a small amount of electrons with higher energies than the potential energy of $N_2(A^3\Sigma_u^+)$.

Guerra and coworkers proposed similar processes, which originated from highly-excited vibrational states of $N_2(X^1\Sigma_g^+)$, for the productions of $N_2(B^3\Pi_g)$, $N_2(C^3\Pi_u)$, and $N_2^+(B^2\Sigma_u^+)$. Reaction (3) is a production process of $N(^2D^o)$. In addition to reaction (3), because of the low excitation energy of 2.38 eV, electron impact excitation

$$N(^4S^o) + e \rightarrow N(^2D^o) + e \quad (5)$$

may contribute more efficiently than reaction (3) for the production of $N(^2D^o)$. The electron energy distribution function in the afterglow, which is calculated by Guerra *et al.*, contains a large amount of electrons with energies higher than 2.38 eV.

The comparison between the experimental results and the aforementioned reaction kinetics suggests that reaction (3) does not dominate the production process of $N_2(A^3\Sigma_u^+)$ and $N(^2D^o)$. This is because reaction (3) produces $N_2(A^3\Sigma_u^+)$ and $N(^2D^o)$ as a pair, while the $N_2(A^3\Sigma_u^+)$ and $N(^2D^o)$ densities had different decay curves as shown in figures 2(a) and 3(a). In other words, it is considered that the dominant production processes for $N_2(A^3\Sigma_u^+)$ and $N(^2D^o)$ are the reactions (2) and (5), respectively. The decay curve of the $N_2(A^3\Sigma_u^+)$ density at 0.5 Torr was rather steep as shown in figure 2(a), while the decay of the $N_2(A^3\Sigma_u^+)$ density at 7 Torr was negligible as shown in figure 3(a). These decay characteristics of the $N_2(A^3\Sigma_u^+)$ density may be dominated by the density distribution of $N_2(X^1\Sigma_g^+, v \geq 10)$. On the other hand, the decay curve of the $N(^2D^o)$ density observed at 0.5 Torr was relatively flat as shown in figure 2(a), while a rapid decrease in the $N(^2D^o)$ density was observed at 7 Torr as shown in figure 3(a). These decay characteristics of the $N(^2D^o)$ density may be due to the spatial distribution of the electron energy distribution function. The different decay characteristics of the $N_2(A^3\Sigma_u^+)$ and $N(^2D^o)$ density are of importance from the application point of view, since it suggests a possibility of selective "pseudo-transportation" to the downstream region in a remote plasma source.

4. Conclusions

In this paper, we have demonstrated that the densities of $N_2(A^3\Sigma_u^+)$ and $N(^2D^o)$ in the downstream region of a remote N_2 plasma source are on the order of $10^{14} - 10^{16}$ m^{-3}. The $N_2(A^3\Sigma_u^+)$ and $N(^2D^o)$ densities in the downstream region were not obtained by the transport from the active discharge region, but it was due to their productions. The experimental results reveal that the reactions (2) and (5) are the dominant production processes of $N_2(A^3\Sigma_u^+)$ and $N(^2D^o)$, respectively. The different production pathways for $N_2(A^3\Sigma_u^+)$ and $N(^2D^o)$ suggest the possibility of selective "pseudo-transportation" to the downstream region in a remote plasma source. The present experimental results support dissociation of NF_3 and dry etching of silicon in a remote N_2 plasma source. It is noted finally that the productions of $N_2(A^3\Sigma_u^+)$ and $N(^2D^o)$ are expected to be unaffected by the injection of NF_3 into the process chamber, since the backward flow of NF_3 toward the quartz tube is negligible because of the fast gas flow of N_2.

References

[1] De Benedictis S, Dilecce G and Simek M 1993 *Chem. Phys.* **178** 547
[2] Eriguchi K and Ono K 2008 *J. Phys. D Appl. Phys.* **41** 024002
[3] Hayashi T, Ishikawa K, Sekine M, Hori M, Kono A and Suu K 2012 *Jpn. J. Appl. Phys.* **51** 026505
[4] Horikawa Y, Kurihara K and Sasaki K 2010 *J. Phys. Conf. Ser.* **227** 012012
[5] Sasaki K, Kawai Y and Kadota K 1997 *Appl. Phys. Lett.* **70** 1375
[6] Sasaki K, Kawai Y and Kadota K 1999 *Rev. Sci. Instrum.* **70** 76
[7] Yamashita T 1979 *J. Chem. Phys.* **70** 4248
[8] Belmontea T, Lefevrea L, Czerwieca T, Michela H and Ricard A 1999 *Thin Solid Films* **341** 27
[9] Boeuf J P and Kunhardt E E 1986 *J. Appl. Phys.* **60** 915
[10] Piper L G 1989 *J. Chem. Phys.* **90** 7087
[11] Slanger T G and Black G 1976 *J. Chem. Phys.* **64** 4442
[12] Lisitsyn V N, Provorov A S and Chebotaev V P 1970 *Opt. Spectrosc.* **29** 119
[13] Barbet A, Sadeghi N and Pebay-Peyroula J C 1975 *J. Phys. B: At . Mol. Phys.* **8** 1776
[14] Sakurai T, Kubota T, Takahara Y, Inoue Y and Hori H 1999 *Jpn. J. Appl. Phys.* **38** L590
[15] Macko P and Sadeghi N 2004 *Plasma Sources Sci. Technol.* **13** 303
[16] Guerra V and Loureiro J 1997 *Plasma Sources Sci. Technol.* **6** 361
[17] Cernogora G 1980 *Chem. Phys. Lett.* **74** 417
[18] Horikawa Y, Kurihara K and Sasaki K 2010 *Jpn. J. Appl. Phys.* **49** 026101
[19] Sadeghi N, Foissac C and Supiot P 2001 *J. Phys. D: Appl. Phys.* **34** 1779
[20] Guerra V, Sa P A and Loureiro J 2004 *Phys. J. Appl. Phys.* **28** 125